

Interference-effects in the laser-induced desorption of small molecules from surfaces: a model study

S. Thiel, T. Klüner^{*}, H.-J. Freund

Fritz-Haber-Institut der Max-Planck-Gesellschaft, Faradayweg 4–6, D-14195 Berlin, Germany

Received 28 January 1998

Abstract

A diabatic treatment of laser-induced desorption of small molecules from surfaces is considered to be an essential step of the theoretical quantum mechanical simulation of a DIET process on an ab initio basis. The consequences of this treatment are investigated especially with respect to the resulting velocity distributions of the desorbing species. The distributions of NO desorbing from nickel oxide surfaces are characterised by a bimodal structure. In our calculations the diabatic coupling between several investigated two-state systems is introduced via the off-diagonal elements of the Hamiltonian, which determines the time evolution of the quantum system. This procedure is the basis for a discussion of the experimentally observed features in the velocity distributions in terms of a coherent diabatic picture. © 1998 Elsevier Science B.V. All rights reserved.

1. Introduction

One essential and well-studied topic in surface photochemistry is the laser-induced desorption of small molecules from well-characterised oxide and metal surfaces [1]. This desorption event is very often induced by electronic transitions, yielding the DIET (desorption induced by electronic transitions) process. In a quantum mechanical picture a simple DIET process generally consists of four steps. First, an initial wave packet is excited by a short laser pulse in the femto- or nanosecond regime. This excited wave packet then evolves under the influence of excited-state potentials. Desorption is then caused by a radiationless transition of this wave packet onto ground-state-like final states, where it evolves until the desorption event is completed [2]. The efficiency of this process, namely the desorption yield, is of course governed by the gradients of the potentials, by the horizontal and vertical shifts of these potentials and by the lifetime of the excited wave packet.

Much work has been done on the theoretical simulation of such processes either in classical or in quantum mechanical approaches. Some of the desirable properties of a dynamical simulation involving electronic transitions are the correct description of electronic coherence, the acceptance of any electronic representation and the application to any number of coupled states [3]. An example of effects caused by electronic coherence is the occurrence of Stueckelberg oscillations [4] that are generated by the existence of at least two different pathways to the same final state [5,6].

^{*} Corresponding author.

These different pathways are due to multiple curve crossing phenomena which are explicitly dealt with in some surface oriented studies such as in Refs. [7,8], while nonadiabatic transitions at potential curve crossings is a subject of a recent review [9].

In this context the Na + I harpooning reaction has to be considered. This reaction has been well modelled [10], reproducing the oscillatory behaviour of the laser-induced fluorescence (LIF) signals of dissociating NaI and NaBr. The oscillations are due to the fact that the representing wave packet alternates between being located on a neutral or ionic potential energy curve. The femtosecond dynamics of the NaI reaction and more elementary concepts in femtochemistry are collected in Ref. [11].

A nice introduction to the connections between time structures and their fourier transforms, as embodied in spectral or momentum distributions of the type presented in this article, can be found in Ref. [12], where gaussian wave packet dynamics with respect to molecular spectroscopy are discussed.

In the context of laser-induced desorption the role of nonadiabatic couplings has also been investigated in a recent study [13].

As extensive studies deal with the calculation of ab initio potential energy surfaces of exemplary oxide systems, on the one hand, [2,14] and several approaches exist to calculate nonadiabatic coupling elements between several electronic states [15], on the other hand, a full quantum mechanical ab initio simulation of the DIET process including oxide surfaces may be approached. Such a parameter-free simulation would first of all consist of the perturbation of the ground-state eigenfunction by a short pulse of the experimental width and intensity. This pulse can be handled theoretically applying methods of solving the time-dependent Schrödinger equation including time-dependent Hamiltonians [16]. After the laser pulse is completed, the system Hamiltonian becomes time independent and the excited wave packet evolves quantum mechanically on the potential energy surfaces under the influence of the nonadiabatic coupling elements which are the off-diagonal elements

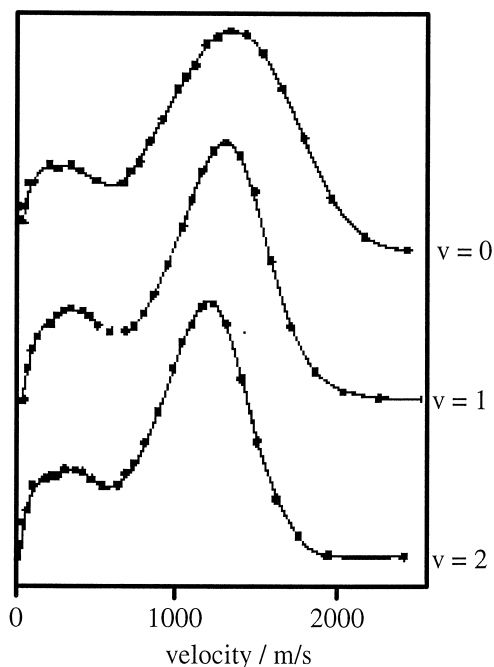


Fig. 1. Velocity distributions of a particular rotational state ($N = 10$) for three vibrational states of the desorbing species. The investigated system was NO ad-sorbed on a thin film of NiO(100) [21].

of the system Hamiltonian. This time evolution can be calculated by quantum mechanical standard methods [17].

In this paper, the consequences of such a diabatic treatment of the DIET process are investigated with respect to the resulting velocity distributions, which are an observable measured for different systems [18–20]. One exemplary set of velocity distributions is plotted in Fig. 1 where the distributions of the particular rotational state $N = 10$ are shown for the three lowest vibrational states. The investigated system was NO being desorbed from a thin NiO(100) film [21].

For comparison, the result of a quantum trajectory approach using a one-dimensional two-state system is first of all presented in Section 2. This treatment is a ‘surface hopping’ approach, which means that the quenching process of the excited wave packet is proceeded by Franck–Condon like vertical wave packet jumps.

2. Quantum trajectory approach

Different kinds of quantum trajectory approaches have been studied in detail for example by Saalfrank [22]. In those studies statistical wave packet jumping methods, very often followed by an incoherent lifetime-averaging procedure, are performed. This means in a simple case that the initial wavefunction ψ_0 is transferred onto the excited state and propagated under the influence of the excited-state Hamiltonian \hat{H}_e for a certain fixed residence lifetime t_e . Then, the excited-state wavefunction is quenched in a Franck–Condon-like manner and propagated on the final-state potential energy surface (with the corresponding Hamiltonian \hat{H}_g) until the desorption probability and the final-state velocity distribution have converged as a function of the final-state propagation time t_g . The final-state wavefunction ψ_g then reads

$$\psi_g(t_g, t_e) = \exp(-i\hat{H}_g t_g) \exp(-i\hat{H}_e t_e) \psi_0 \quad (1)$$

Any observables $A(t_e)$ can then be calculated as a function of the excited-state residence lifetime t_e . Finally, an excited-state lifetime distribution $f(t_e)$ can be assumed, which allows for the calculation of the lifetime averaged observable \bar{A} . In the example presented at this stage, an exponential decay of the excited-state

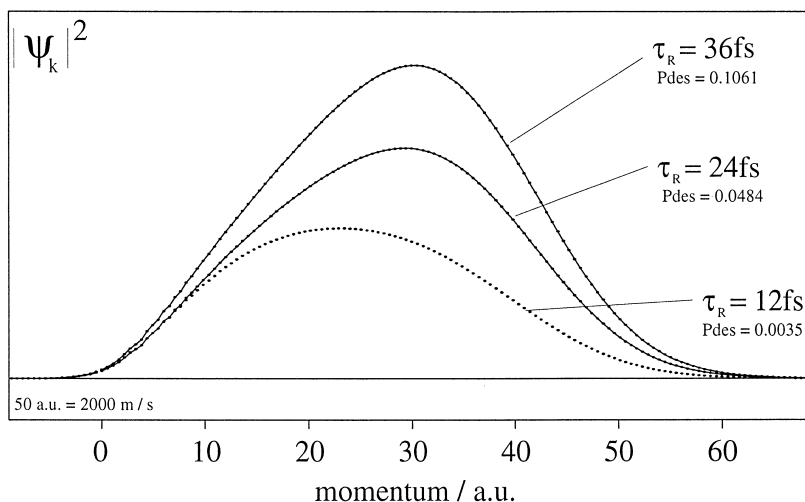


Fig. 2. Lifetime-averaged velocity distributions of NO for three different resonance lifetimes τ_R . These distributions are the result of the quantum-trajectory approach described in the text. Indicated are the weighted desorption probabilities $P_{\text{des}}(\tau_R)$.

population is used, which yields the weighting procedure proposed by Gadzuk [23]. In his approach, the averaged observable \bar{A} is calculated as a function of the resonance lifetime τ_R .

$$\begin{aligned}\bar{A}(\tau_R) &= \frac{\int_0^\infty f(t_e, \tau_R) A(t_e) dt_e}{\int_0^\infty f(t, \tau_R) dt_e} \\ &= \frac{\int_0^\infty \exp(-t_e/\tau_R) A(t_e) dt_e}{\int_0^\infty \exp(-t_e/\tau_R) dt_e}\end{aligned}\quad (2)$$

The observable which is focused upon in this approach is the final-state velocity or momentum distribution, i.e. the momentum-space probability density of the desorbed part of the wavefunction. In order to present the result of such a ‘surface hopping’ approach, we have used a PES configuration resulting from extensive ab initio calculations for the NO/NiO(100) system performed in our group [24]. Applying Eq. (2) to this momentum-space probability density yields the distributions shown in Fig. 2 for three different resonance lifetimes τ_R . The distributions are monotonous and monomodal, as expected from this one-dimensional treatment [2,25]. The values for the weighted desorption probabilities are given in Fig. 2.

3. Diabatic approach

All of the presented diabatic simulations follow the scheme of Fig. 3. This scheme contrasts the quantum trajectory approaches because the representing wave packet is not propagated under the influence of the excited-state Hamiltonian for certain fixed residence lifetimes, but it evolves on both potential energy curves of our one-dimensional two-state system coherently. This means that the total nuclear wavefunction

$$\Psi = \begin{pmatrix} \psi_1 \\ \psi_2 \end{pmatrix}\quad (3)$$

evolves in each single time step under the influence of the Hamiltonian matrix \hat{H} :

$$\hat{H} = \begin{pmatrix} \hat{H}_{11} & \hat{V}_{12} \\ \hat{V}_{21} & \hat{H}_{22} \end{pmatrix}\quad (4)$$

The diagonal elements of this matrix are the Hamiltonians of the two single diabatic potential energy surfaces, while the diabatic coupling between these surfaces is included via the coupling operators, which are the off-diagonal elements of the matrix (4). Throughout this study gaussian coupling functions are used, as indicated in Fig. 3.

A typical result of such a wave packet simulation using one-dimensional semi-empirical potentials (for the parameters of all diabatic simulations see Appendix A) is presented in Fig. 4a. Shown is the probability density in momentum-space on the final state after a total simulation time of 720 fs. At this time the relaxation event can certainly be considered to be complete, because the final-state square norm has converged as a function of the propagation time t , as shown in Fig. 4b. Concerning the diabatic coupling function, a gaussian has been chosen, which is located near the crossing point, slightly shifted towards the repulsive region of the two potential curves. The width and intensity of the function were chosen to account for a high final-state square norm, which makes the analysis of the velocity distribution easier. However, because of the large absolute value

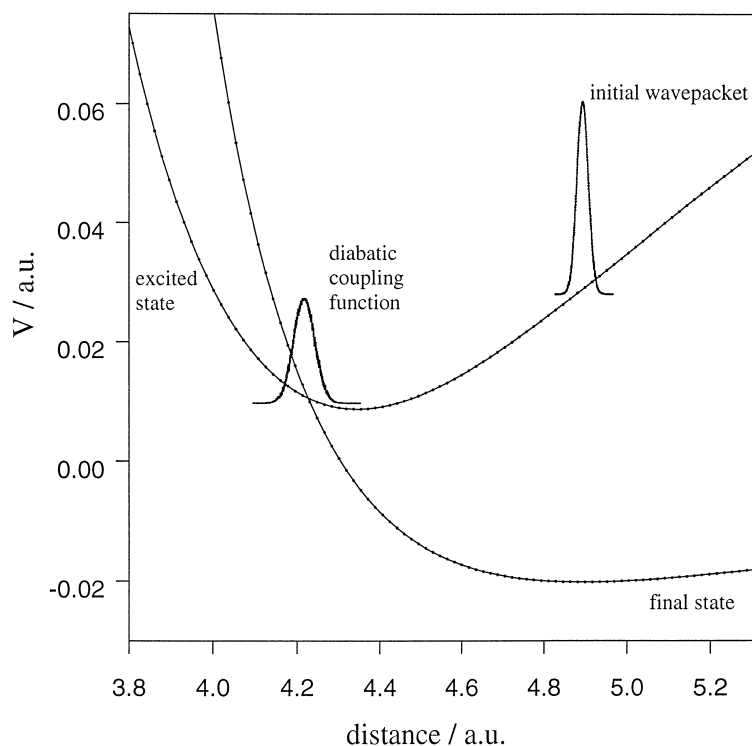


Fig. 3. Scheme of the diabatic simulations. An initial wave packet has been transferred onto the excited state in a Franck–Condon-like manner.

of the coupling function a direct comparison with experimental observables such as desorption probability should be regarded with some caution.

The density in momentum-space on the final state is interpreted as the momentum distribution of the desorbing NO molecules. This distribution differs drastically from the monomodal distributions one usually gets in any one-dimensional wave packet jumping scenario [25], as was shown in the previous section. For this reason, the remainder of this paper consists of several simplified model calculations, which demonstrate the origin of the presented features of the exemplary velocity distribution shown in Fig. 4a.

However, first, another velocity distribution is presented. In Fig. 4c the result of the same calculation as in Fig. 4a is shown, but in this case the coupling was ‘turned off’ after one complete oscillation of the wave packet in the initial state. This corresponds to a sudden extinction of the coherence between the two states. The resulting distribution shows clearly less pronounced features, but the main features of the distribution in Fig. 4a are already visible, especially considering the integral intensity. This is proofed by presenting both distributions in a common plot as is done in Fig. 4d. This means that the final-state velocity distribution resulting after one oscillation of the wave packet in the excited state can be regarded as kind of representative for a distribution resulting from a full coherent calculation. Of course it has to be kept in mind that the very pronounced features in Fig. 4a are also a result of the low dimensionality of this treatment. It is expected that these features are partly washed out if the number of degrees of freedom is increased.

As mentioned before, the following section of this paper is devoted to demonstrating the origins of the essential features of a momentum-space distribution resulting from a diabatic treatment of the laser-induced desorption process.

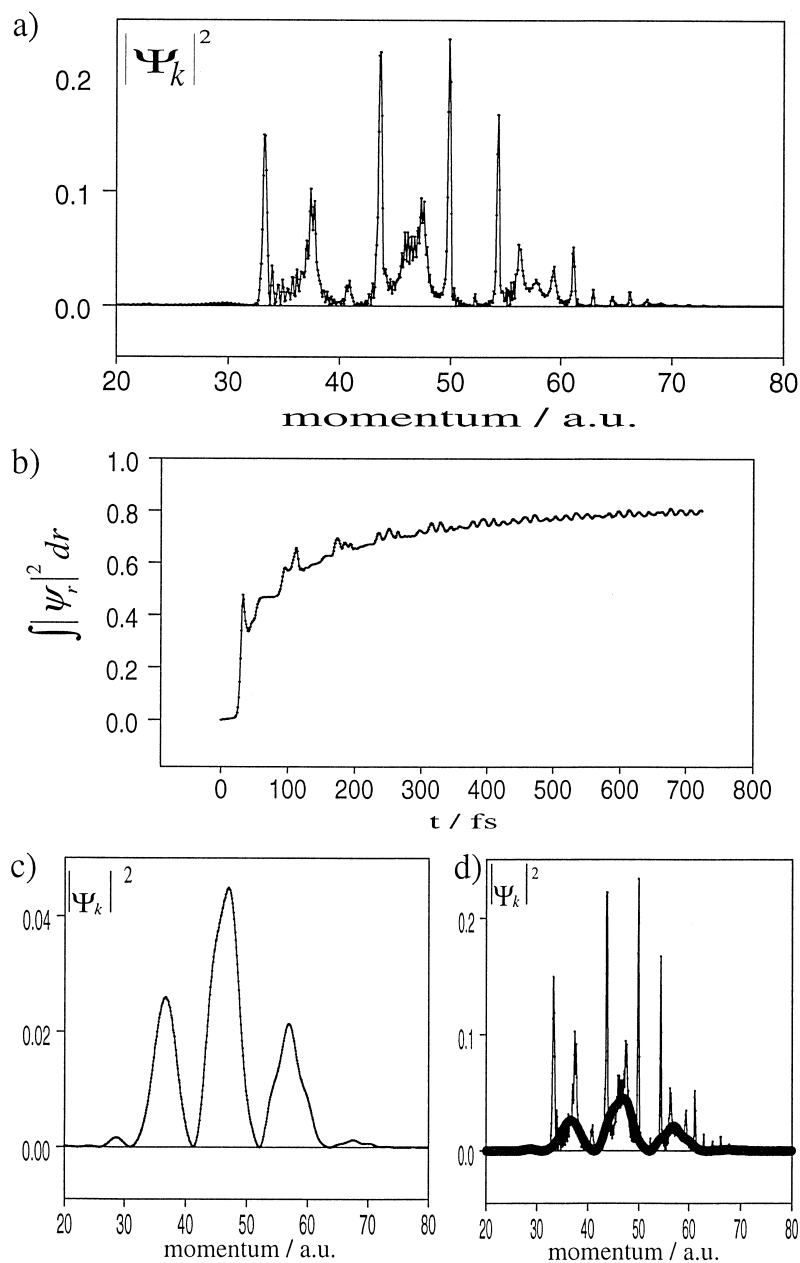


Fig. 4. (a) Final-state momentum space density after 720 fs. (b) Final-state square norm as a function of propagation time. (c) Final-state momentum space density after 720 fs with the coupling being 'turned off' after one oscillation of the initial wave packet in the excited state. (d) Common plot of the distributions shown in (a) and (c).

3.1. Model calculations on simple one-dimensional potentials

In this section two simple one-dimensional potential configurations are considered. At the beginning the calculations are restricted to a time duration of one complete oscillation of the wave packet in the initial state,

because up to this time the resulting features in the velocity distributions on the final state can be understood quite easily. The excited (initial) states are harmonic oscillators for simplicity while purely repulsive final states are used. These repulsive final states were chosen, because oscillations of partial wave packets on the final-state potential, accompanied by possible back transfers to the originally initial state are avoided.

3.1.1. Special case of a configuration with identical potentials in the repulsive region

Fig. 5a shows a configuration where the repulsive regions of both potential curves overlap exactly. The diabatic coupling function is localised at the minimum of the excited-state harmonic oscillator potential.

Generally, in typical diabatic calculations with a realistic potential curve configuration the initial wave packet crosses a diabatic crossing between the initial state and the final state twice in the early stage of the desorption

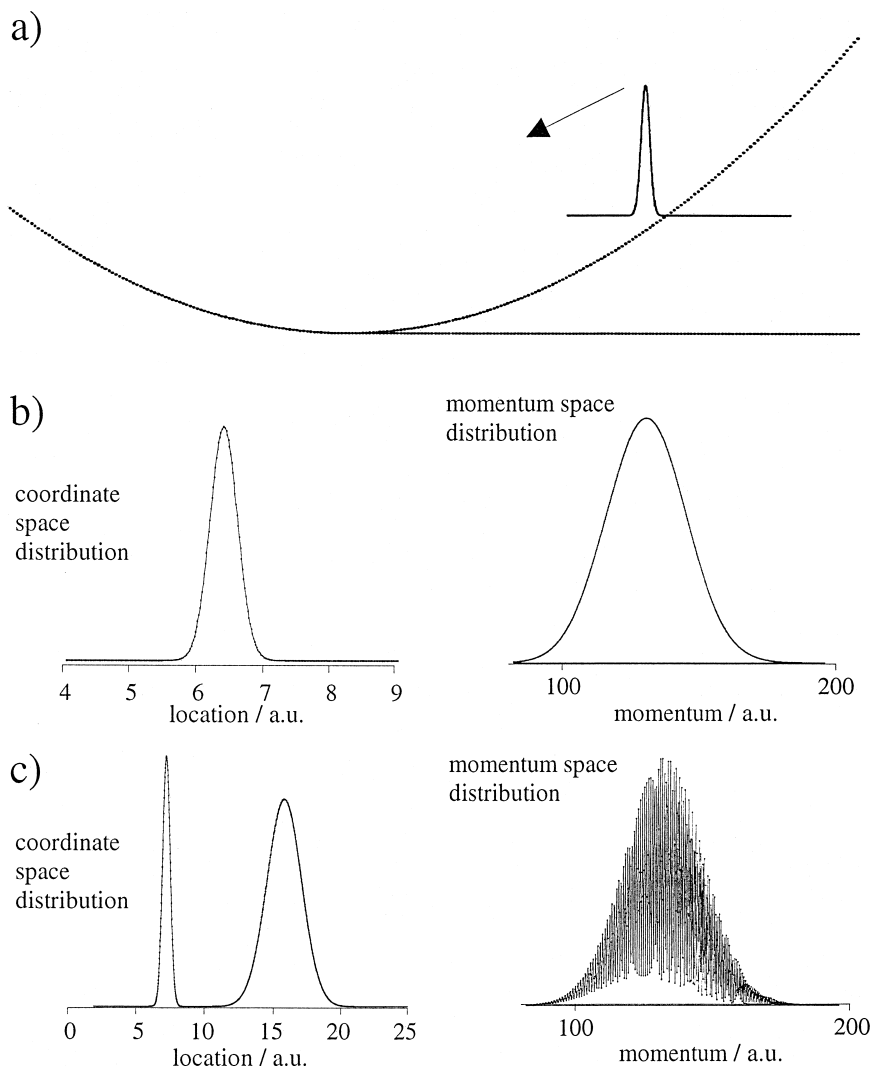


Fig. 5. Special case of a configuration with identical potentials in the repulsive region: (a) initial configuration; (b) coordinate and momentum-space distributions after one oscillation of the initial wave packet in the excited state; (c) coordinate- and momentum-space distributions after two oscillations of the initial wave packet in the excited state.

event. The first crossing happens during the first half-period of the oscillation in the excited state and splits the initial wave packet into two partial wave packets which are localised on two different potential curves then. The second crossing happens when the split partial wave packets return towards the initial position after reaching the turning points of their oscillation. During this second event, both partial wave packets transfer a part of themselves onto the other state again and the oscillation is completed. To summarise, during the first oscillation two partial wave packets are transferred onto the final state and are interfering on this state. As in the case of Fig. 5a both partial wave packets have passed the same distance before interfering on the final state, no difference in phase of the wavefunctions exists and no features in the final-state distribution can be seen in coordinate- and momentum-space. The calculated final-state distributions for the example of Fig. 5a after one oscillation of the initial wave packet in the excited state are shown in Fig. 5b. The consequences of a difference in the pathway of two interfering partial wave packets are presented in the following subsections.

Interesting in this example are the resulting final-state distributions after the second oscillation of the wave packet in the excited state. As shown in Fig. 5c, the repetition of the first event produces a second wave packet in coordinate-space on the final state which shows no features or oscillations as well. The first wave packet, resulting from the first oscillation in the excited state has moved further in positive x -direction on the final state and is spread. The corresponding momentum distribution shows many oscillations due to the large difference in pathway between the partial wave packets in coordinate-space which is a result of the second oscillation of the initial wave packet in the excited state.

To summarise this short section, the fine structure in the momentum-space distribution of this example is caused by the time delay of the second partial wave packet which is on the order of magnitude of one oscillation period in the initial state.

3.1.2. Configuration with non-identical potentials in the repulsive region

This example deals with the configuration presented in Fig. 6a. The repulsive region of the final-state potential of Fig. 5a was modified in order to impose a difference in pathway between partial wave packets after crossing the diabatic coupling for the first time during the first oscillation of the initial wave packet in the excited state. So two different kinds of features in the final-state velocity distributions are combined in this investigation.

Fig. 6b shows the final-state distributions in coordinate-space and momentum-space after one oscillation in the excited state. Due to the different pathways the partial wave packets have moved this time during this first oscillation before interfering on the final state, the momentum-space distribution is characterised by some slight oscillations. Of course the two different path lengths are caused by the difference in the gradients of the potential curves in the region behind the crossing point, contrasting the situation of Fig. 5a. As the pathway difference is small in this example, the wave packets are not clearly separated in coordinate-space and interference is visible here as well. A detailed analysis, which is not presented in this context, has revealed that the two peaks in the velocity distribution do not correspond to the two peaks in the coordinate-space distribution separately, as one could guess at a first glance.

The result of the second oscillation in the excited state (Fig. 6c) is a superimposition of a fine structure onto the momentum-space distribution resulting from one oscillation. These new features are again characterised by the pathway difference that is due to the oscillation period of the wave packet in the excited state as in the example of the last subsection.

Comparing Fig. 6b,c one sees that the picture in momentum-space after one oscillation of the initial wave packet in the excited state is the envelope of the distribution one gets after the second oscillation. This effect can directly be compared with the observation at the very beginning namely that one oscillation yields a velocity distribution which is already kind of representative for the distribution after a full coherent diabatic wave packet simulation using realistic potentials. As the resulting features become more and more complicated the investigation of an increased number of oscillations using realistic potentials will not be approached here.

Furthermore, the rapid oscillatory effects caused by more than one oscillation of the initial wave packet in the

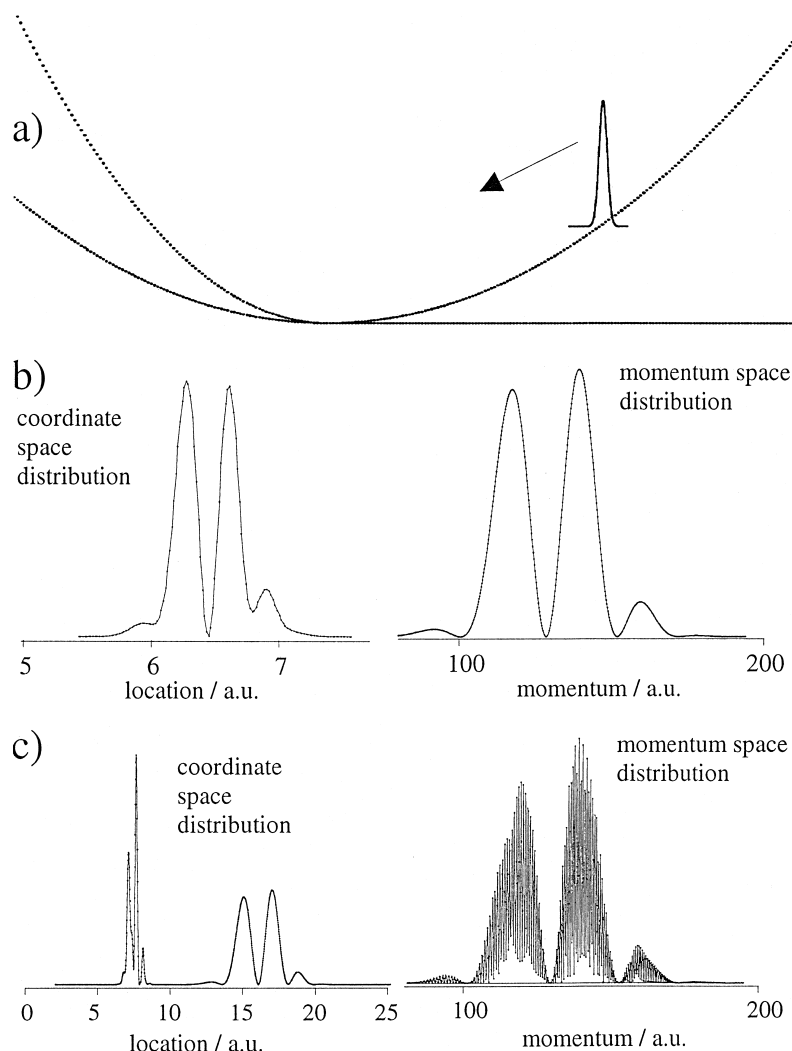


Fig. 6. Configuration with non-identical potentials in the repulsive region: (a) initial configuration; (b) coordinate- and momentum-space distributions after one oscillation of the initial wave packet in the excited state; (c) coordinate and momentum-space distributions after two oscillations of the initial wave packet in the excited state.

excited state can be assigned as a long time phenomenon which is not likely to be of any experimental importance in a surface or condensed matter environment.

3.2. Role of the coupling function

All of the diabatic wave packet simulations presented in this study used empirical gaussians as coupling functions. In this section some principle aspects of the coupling functions referring to the desorption probability are investigated. A more detailed analysis of diabatically coupled systems for example with respect to the transition probability is given in a recent study [26] using a system consisting of two diabatically coupled harmonic oscillators. With the configuration sketched in Fig. 7a it is demonstrated that the effects of a variation in the coupling function parameters are pronounced.

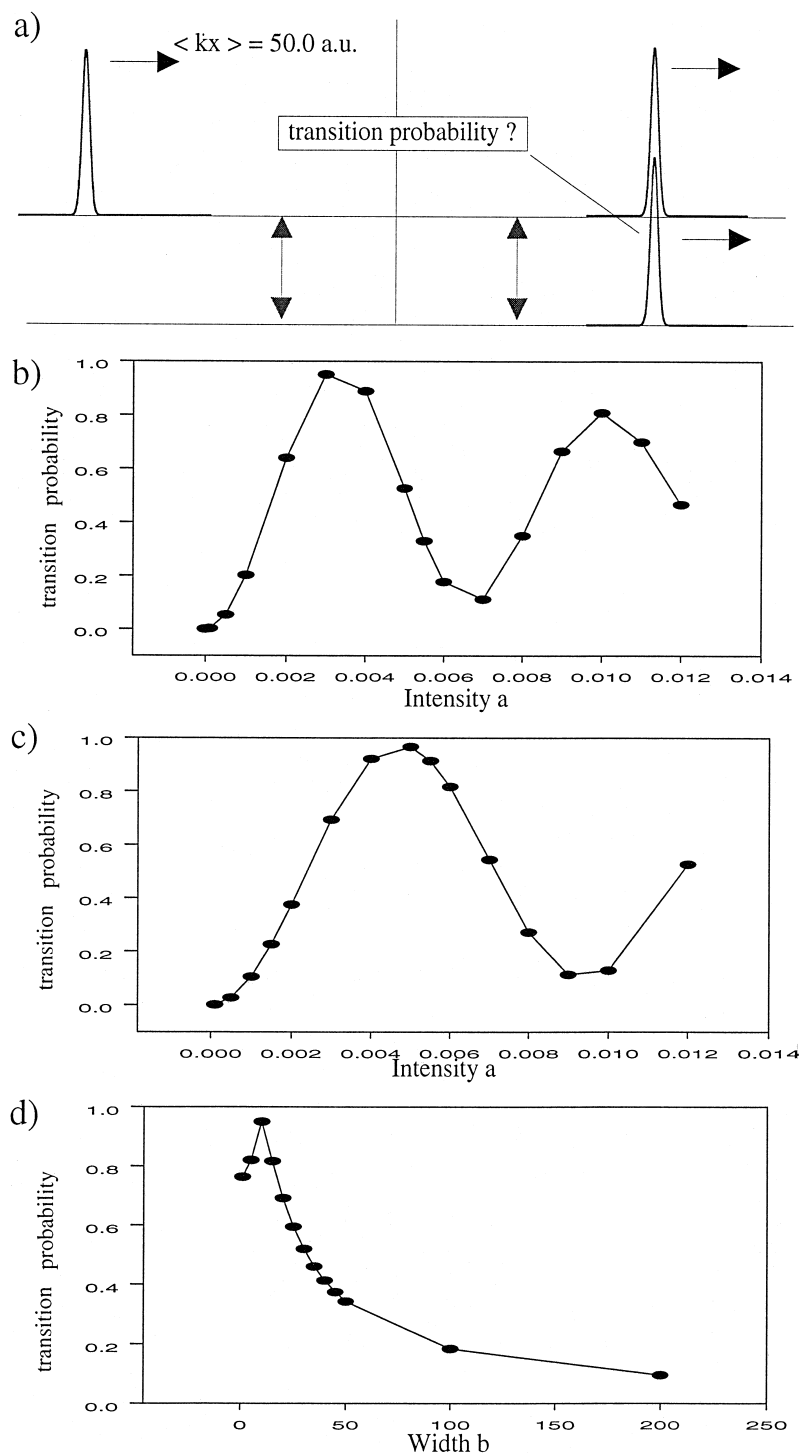


Fig. 7. The role of the coupling function: (a) configuration before and after the crossing event; (b) transition probability as a function of the parameter a for $b = 10$; (c) transition probability as a function of the parameter a for $b = 20$; (d) transition probability as a function of the parameter b for $a = 0.003$.

The initial wave packet simulates a free particle having the mass of an NO molecule and moving uniformly with a momentum of 50 au along positive x -direction. Reaching a region, where a coupling between the two states ($V = 0$ in both cases) exists, this wave packet splits and a partial wave packet is transferred onto the final state, where its uniform translation continues. The square norm of this transferred partial wave packet is considered in this study as the transition probability of the coupling function which has the general expression:

$$v_{\text{diab}} = a \exp(-b(x - x_0)^2) \quad (5)$$

Fig. 7b–d show the dependence of the transition probability on the parameters a and b in Eq. (5). Remarkable is the oscillatory behaviour of this transition probability as a function of the intensity parameter a in case of two different fixed values for b in Fig. 7b,c, respectively. The non-monotonous course in Fig. 7d, where b is varied for a constant intensity is not easy to interpret as well. A further investigation of these facts will not be done in this approach, but it has to be emphasised that the coupling function has a remarkable influence on observable quantities as for example the desorption probability in more realistic wave packet simulations. The problem of nonadiabatic transition probabilities has been solved in closed analytical form for many one-dimensional model systems by Nakamura [9].

4. Discussion

After finishing the previously presented model studies, the final-state velocity distribution shown in Fig. 4a is reconsidered. Due to the fact that the features of this calculated velocity distribution cannot be experimentally resolved, the possibility of a convolution procedure has to be taken into account. For this reason every single point of the momentum-space distribution is multiplied with a gaussian followed by summing up the results at each grid point. Of course the choice of the parameter w in expression (6) for the convolution function is most important concerning the resulting convoluted distribution.

$$g(w, k) = N \exp\left(-\frac{(k - k_0)^2}{w^2}\right) \quad (6)$$

with N being a normalisation constant and k_0 the grid point in momentum-space where $g(w, k)$ is applied.

Fig. 8 shows the distribution presented in Fig. 4a, convoluted with four different parameters w . Especially the velocity distributions in Fig. 8c,d, where the convolution parameter is on the order of magnitude of experimental resolution are quite well comparable to experimentally observed distributions [19,20]. For this reason, the experimentally observed structure in velocity distributions may be discussed in terms of a pure interference effect between partial wave packets. These partial wave packets have been transferred to the final state of the investigated two-state systems by curve crossing events. The sharp lines and the heavy oscillations in the momentum distributions have been shown to be caused by at least two oscillations of the initial wave packet in the excited state. Comparing with typical experimental distributions [20], one has to argue that the consequences of more than one oscillation are absent, because dissipation takes a part. Still the bimodality in velocity distributions could be caused by a single curve crossing event as it seems reasonable for example by inspection of Fig. 6b. At this stage the importance and physical significance of the smooth envelope enclosing the rapid oscillatory structure and not the unobservable fine points of the oscillations should be emphasised.

Of course, one should keep in mind that a more realistic approach should consider a final-state manifold including more than one degree of freedom. However, this is beyond the scope of the present study, since the examples of this paper should be regarded as a qualitative explanation of the importance of nonadiabatic couplings between potential energy surfaces. A multi-state model would leave our conclusions concerning the

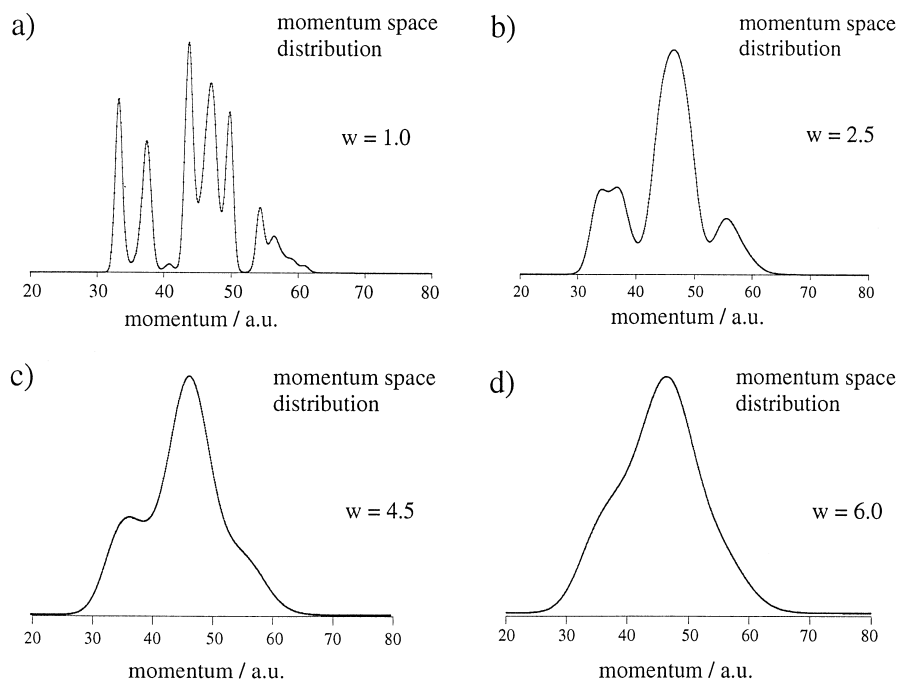


Fig. 8. Convolution of the momentum-space distribution shown in Fig. 4a. Four different convolution parameters were used.

occurrence of interference generally untouched. Furthermore, the description of the origin of the different features in the velocity distributions was most understandable within the simple two-state models. The general occurrence of interference should also be independent of the particular shape of the coupling function. Of course, details of the final-state distributions will definitely depend on the parameters of the coupling function.

In order to check our conclusions, the velocity distributions resulting from a pump-probe experiment could be measured. This pump-probe experiment should be designed in such a way that very shortly after the initial laser pulse, which transfers the initial wave packet onto an excited state, the coherence between the participating states is disturbed by a second laser pulse. This extinction of coherence should have influence on the final-state velocity distribution, as interference between partial wave packets is avoided or at least changed.

Concluding, we have investigated the consequences of a diabatic treatment of laser-induced desorption of small molecules from surfaces on the velocity distribution of the desorbing species. The features in the resulting momentum-space densities were separately traced back to different kinds of pathway differences between interfering partial wave packets. In order to figure out the origin of these features, very simple model configurations were considered. It seems possible that the observed features in the experimental velocity distributions are caused by interference of partial wave packets being generated by curve crossing events.

Acknowledgements

The work was financially supported by the Deutsche Forschungsgemeinschaft through the Graduiertenkolleg 'Dynamische Prozesse an Festkörperoberflächen' and by the German–Israeli Foundation (GIF). We would like to thank R. Kosloff and V. Staemmler for many helpful and stimulating discussions.

Appendix A. Parameters of the diabatic wave packet calculations

In all diabatic wave packet simulations the time evolution of the initial wavefunction $\psi(t) = \hat{U}(t)\psi(t=0)$ has been calculated by a Newtonian polynomial algorithm [28]. The parameters of the calculations are the grid range $[x_{\min}, x_{\max}]$, the number of grid points npx, the time step Δt , the total number of time steps (# steps), the number of interpolation points within the polynomial algorithm and the mass m of the particle. Furthermore, the initial wavefunction is given which is normalised and located on the potential curve assigned with the index 2 at the beginning of the simulations [27].

figure 4:

$x_{\min}=3$ au	$x_{\max}=75$ au	npx=4096
$\Delta t=50$ au	interpolation points=256	$m=54686.649$ au # steps = 1000
	initial state:	$\Psi_{02} = \exp(-10 \cdot (x - 4.7)^2)$ (normalised)
coupling:	$v_{diab} = 0.1 \cdot \exp(-25.5 \cdot (x - 3.9)^2)$	or $v_{diab} = 0$ after 67 time steps
potentials:	$V_2(r) = 0.294au - 1.2au/r + 0.02019au \cdot [\exp(-1.2189/au \cdot (r - 4.8au))]$	
	$\cdot [[\exp(-1.2189/au \cdot (r - 4.8au))] - 2]$	
	$V_1(r) =$ ground state potential from [27] for $\theta = 45^\circ$	

figures 5, 6:

$x_{\min}=1.9$ au	$x_{\max}=35$ au	npx=2048
$\Delta t=100$ au	interpolation points=128	$m=54686.649$ au # steps = 35 for 1 oscillation = 75 for 2 oscillations
	initial state:	$\Psi_{02} = \exp(-10 \cdot (x - 6.0)^2)$ (normalised)
coupling:	$v_{diab} = 0.003 \cdot \exp(-10 \cdot (x - 4.6)^2)$	
potentials:	$V_2 = 0.08 \cdot (x - 4.6)^2$	
figure 5:	$V_1 = 0.08 \cdot (x - 4.6)^2$	$x < 4.6$
	$V_1 = 0$	else
figure 6:	$V_1 = 0.09 \cdot (x - 4.6)^2$	$x < 4.6$
	$V_1 = 0$	else

figure 7:

$x_{\min} = -4$ au	$x_{\max} = 10$ au	npx=1024
$\Delta t=50$ au	interpolation points=128	$m=54686.649$ au # steps=100
initial state:	$\Psi_{02} = \exp(-25 \cdot (x + 2)^2) \cdot \exp(i \cdot x \cdot 50.0)$ (normalised)	
potentials:	$V_1 = 0$	
	$V_2 = 0$	

References

- [1] F.M. Zimmermann, W. Ho, Surf. Sci. Rep. 22 (1995) 127.
- [2] T. Klüner, H.-J. Freund, J. Freitag, V. Staemmler, J. Chem. Phys. 104 (1996) 10030.
- [3] J.C. Tully, J. Chem. Phys. 93 (1990) 1061.

- [4] E.C.G. Stückelberg, *Helv. Phys. Acta* 5 (1932) 369.
- [5] E.E. Nikitin, *Theory of Elementary Atomic and Molecular Processes in Gases* (Clarendon, Oxford, 1974).
- [6] M.S. Child, *Atom-Molecule Collision Theory*, in: R.B. Bernstein (Ed.) (Plenum, New York, 1979).
- [7] J.W. Gadzuk, *Surf. Sci.* 118 (1982) 180.
- [8] J.W. Gadzuk, J.K. Norskov, *J. Chem. Phys.* 81 (1984) 2828.
- [9] H. Nakamura, *Annu. Rev. Phys. Chem.* 48 (1997) 299.
- [10] V. Engel, H. Metiu, R. Almeida, R.A. Marcus, A.H. Zewail, *Chem. Phys. Lett.* 152 (1988) 1.
- [11] J. Manz, L. Wöste (Eds.), *Femtosecond Chemistry* (VCH, Weinheim, 1995).
- [12] E.J. Heller, *Acc. Chem. Res.* 14 (1981) 368.
- [13] H. Aizawa, S. Tsuneyuki, *Surf. Sci.* 377 (1997) 610.
- [14] T. Klüner, H.-J. Freund, J. Freitag, V. Staemmler, *J. Mol. Catal. A* 119 (1997) 155.
- [15] T. Pacher, L.S. Cederbaum, H. Köppel, in: I. Prigogine, S.A. Rice (Eds.), *Advances in Chemical Physics*, Vol. LXXXIV (John Wiley, New York, 1993).
- [16] U. Peskin, R. Kosloff, N. Moiseyev, *J. Chem. Phys.* 100 (1994) 8849.
- [17] R. Kosloff, *J. Phys. Chem.* 92 (1988) 2087.
- [18] K. Fukutani, M.-B. Song, Y. Murata, *J. Chem. Phys.* 103 (1995) 2221.
- [19] G. Eichhorn, M. Richter, K. Al-Shamery, H. Zacharias, *Proceedings of the SPIES, OE/Laser 98 Conference* (in press).
- [20] M. Menges, B. Baumeister, K. Al-Shamery, H.-J. Freund, C. Fischer, P. Andresen, *J. Chem. Phys.* 101 (1994) 3318.
- [21] Th. Mull, B. Baumeister, M. Menges, H.-J. Freund, D. Weide, C. Fischer, P. Andresen, *J. Chem. Phys.* 96 (1992) 7108.
- [22] P. Saalfrank, *Chem. Phys.* 211 (1996) 265.
- [23] J.W. Gadzuk, *Surf. Sci.* 342 (1995) 345.
- [24] T. Klüner, H.-J. Freund, V. Staemmler, R. Kosloff, *Phys. Rev. Lett.* 80 (1998) 5208.
- [25] S. Thiel, T. Klüner, M. Wilde, K. Al-Shamery, H.-J. Freund, *Chem. Phys.* 228 (1998) 185.
- [26] A. Ferretti, A. Lami, G. Villani, *J. Chem. Phys.* 106 (1997) 934.
- [27] B. Baumeister, H.-J. Freund, *J. Phys. Chem.* 98 (1994) 11962.
- [28] R. Kosloff, *Annu. Rev. Phys. Chem.* 45 (1994) 145.